



Simulation study of an air-gap membrane distillation system for seawater desalination using solar energy

Abdelfatah Marni Sandid^{a,b,*}, Taeib Nehari^{a,b}, Driss Nehari^a

^aDepartment of Mechanical Engineering, University of Ain Temouchent, 46000 Ain Temouchent, Algeria, emails: abdelfatahsandid@hotmail.com (A. Marni Sandid), nehari_tb@yahoo.fr (T. Nehari), and nehari2746@gmail.com (D. Nehari)

^bSmart Structures Laboratory (SSL), University of Ain Temouchent, 46000 Ain Temouchent, Algeria

Received 11 January 2021; Accepted 6 May 2021

ABSTRACT

The paper presents a numerical study to investigate the solar membrane distillation (SMD) system for seawater desalination using solar energy. The SMD system includes both flat plate collectors and photovoltaic panels. Therefore, the photovoltaic system is used to power electrically the pumps and sensors. The present model has good compatibility of no more than 5% with the experimental air-gap membrane distillation (AGMD) system. It was found that the solar AGMD system is used for the production of 3–5 L/h of distilled water flow. In addition, the energy needed is calculated for the pumps and replaced by two photovoltaic panels, each one has an area of 1.6 m² using an energy storage battery (12 V, 200 Ah). Besides, the brine that contains the high salt concentration is completely dispensed with this process. Therefore, the energy efficiency of the AGMD module and the collector efficiency values reach 68% and 74% respectively. The solar AGMD system will be studied using TRNSYS and PVGIS programs on different days throughout the year in Ain Temouchent weather, Algeria.

Keywords: Solar desalination; Membrane distillation; Photovoltaic system; Solar-thermal system; Seawater

1. Introduction

Population growth and the degradation of some freshwater resources are two problems that make us look for developing modern technologies for water desalination. In many countries and places across the world, seawater is used in desalination processes because it covers a large area of 70% of the land. The reverse osmosis technology has been used that provides a large flow of freshwater; however, it also consumes large electrical energy due to the use of huge pumps in this technology [1]. Therefore, the membrane distillation (MD) process has been used for seawater desalination. The MD processes are used at low temperatures and less than 100°C. Therefore, more efficient

methods have been used for the desalination process due to 100% salt rejection with low fouling and operating pressure in MD applications [2].

Membrane distillation is a thermal process in which water vapor is transported through a hydrophobic porous membrane. The liquid phase to be treated must be kept in contact with one face of the membrane without penetrating its pores unless the transmembrane pressure is greater than the inlet pressure. The hydrophobicity of the membrane prevents liquid from entering the pores thanks to the surface tension. Thus, liquid/vapor interfaces are created near the pores. There are several types of membrane distillations. The differences only concern the permeate side and will condition the driving force of the separation.

* Corresponding author.

Until now, polytetrafluoroethylene (PTFE), polyvinylidene fluoride, polyethylene, and polypropylene have been the most commonly used membranes for MD processes [3].

There are four main configurations of membrane distillation modules in the literature [4,5–7]: direct contact membrane distillation (DCMD), air-gap membrane distillation (AGMD), sweeping gas membrane distillation (SGMD), and vacuum membrane distillation (VMD). This difference in the nature of the permeate treatment: the condensation of the vapor that has passed through the membrane takes place inside the module for DCMD and AGMD configurations and outside the module for VMD and SGMD configurations. DCMD is the most MD configuration technology studied due to the simplicity and ease of handling, where its energy efficiency, called the membrane thermal efficiency (MTE), is commonly related to the operating conditions [8]. In the MD process field, the DCMD process has a lower MTE against the AGMD procedure because of conduction heat losses. The mechanism functions of the AGMD systems are based on the stagnant air gap interposition between the membrane and condensation area, which leads to an inherently increase in the thermal energy efficiency of the process [9]. Consequently, the first patent to discuss the principle of AGMD appeared with Hassler [10] and Weyl [11] for the basic knowledge, in which the concept and behavior of AGMD systems can be found in different literature studies [12–14].

According to the high-energy costs associated with existing desalination methods, there is a great demand for technologies that can use low-temperature sources like waste heat or solar energy. Although recent developments in AGMD configurations, the first flat plate AGMD system was developed by the Swedish Svenska Utvecklings AB in 2016 [15], while such modules today are manufactured and commercialized by Scarab Development. Each module is made up of 10 planar cassettes with an overall membrane surface of 2.3 m² and a global capacity of 1–2 m³/d of distillate water [16]. The single-stage consists of injection-molded plastic frames containing two parallel membranes, feed and exit channels for warm water, and two condensing walls [15,17].

On the other hand, Khan and Martin [18] conducted experimental analysis from arsenic removal using single cassette AGMD with an effective membrane area of 0.2 m² and reported fluxes of 20 L/m²h at a temperature difference of 50°C between hot and cold inlet temperatures. He et al. [19] applied factorial design and response surface methodology (RSM) to analyze the relationships between operating parameters (hot and cold inlet temperatures, feed flow rate) on performance indicators including distillate flux and gained output index of a hollow fiber AGMD module.

In Kumar and Martin's work [20], a single cassette AGMD module is characterized to identify the effect of process parameters on distillate flux and thermal efficiency. Favorable conditions to obtain a distillate flow rate of 3–5 kg/h determined on a bench-scale experimental setup. The developed RSM regression model was tested by analysis of variance and studied using experimental results of Asim et al. [21]. Parametric optimization was carried out as well to identify suitable conditions for operating MD with constant or dynamic energy supply (e.g., solar

thermal energy). Then, experiments on a solar membrane distillation (SMD) system were carried out in October during which maximum radiation would be incident on solar collectors installed in the United Arab Emirates.

Dynamic simulation of the combined system using tools such as TRNSYS and parametric analysis enables to design of a functional system and then optimizes it. In this study of Kumar and Martin [22], the application of the cogeneration system for residential households in the UAE is considered for per capita production of 4 L/d of pure water and 50 L/d of domestic hot water. The optimized cogeneration system utilizes more than 80% of the available solar energy gain and operates at 45% and 60% collector efficiencies for flat plate collectors (FPC) and ETC systems respectively. The cogeneration operation reduces 6%–16% of thermal energy demand and also enables 25% savings in electrical energy demand. In Gowtham's paper [23], a novel solar thermal polygeneration (STP) system for the production of cooling, clean water, and domestic hot water is modeled and analyzed for the weather conditions of the UAE using TRNSYS software. The system comprises solar collectors for the production of thermal energy. Economic benefits are analyzed for different collectors and fuel costs savings. The lowest payback period of 6.75 y is achieved by STP with evacuated tube collector field having a gross area of 216 m².

The configuration studied in this article for seawater desalination is AGMD. It is a thermal membrane process, the driving force behind the transfer being a partial pressure difference on either side of the membrane created by a temperature difference. Compared to other membrane distillation techniques, AGMD seems interesting for its aspects of low membrane wetting and the fact that there is no additional energy consumption linked to the use of an additional pump. In recent years, AGMD has experienced more sustained development, mainly in research, thanks to developments in membrane manufacturing techniques. Seawater desalination is one of the most promising fields for the application of solar thermal energy due to the coincidence, in many places of the world, of water scarcity, seawater availability, and good levels of solar radiation (like Algeria). The SMD is recently an under-investigation desalination process suitable for developing self-sufficient small-scale applications. The use of solar energy considerably reduces operating costs.

The main objective of this project is to analyze and optimize renewable-driven AGMD systems. This objective can contribute to ensuring the availability of distillate water using the solar desalination process. In this paper, a numerical model of desalination that depends on single cassette AGMD module integrated solar thermal system is validated with simulation results of Kumar and Martin [20] which was carried out an experimental study on SMD system only in October on solar collectors installed in the UAE as previously mentioned. Then, a solar AGMD system is studied for optimizing the operation of a SMD, in terms of thermal efficiency, distillate production, and cost savings. Besides, the brine that contains the high salt concentration is completely dispensed with this process. Therefore, a TRNSYS program [24] and PVGIS software [25] are used to predict the long-term performance of the solar AGMD system at different

times throughout the year in Ain Temouchent weather, Algeria.

2. Description: the AGMD system

Fig. 1 shows a schematic presentation of the principle of the seawater air-gap membrane desalination process using solar energy. The three major components in the solar AGMD system are a solar-thermal system, a solar photovoltaic (PV) system, and an AGMD unit.

2.1. Solar-thermal system

The studied system contains the thermal energy loop, as shown in Fig. 1. The system incorporates five FPC with a total area of 12.75 m² with a controller, a counter-flow heat exchanger, a controller in differential temperature, and pumps. The water flow rate is controlled by an ON/OFF controller to optimize thermal energy harvesting and setting time. Due to the convergence of climatic changes between Algeria and the UAE, we chose five flat plate collectors in order to obtain a suitable temperature to provide a flow rate of 5 L/h of distilled water in the weather of the state Ain Temouchent (latitude 35°3'0" N, longitude 1°1'0" E), Algeria.

2.2. Solar photovoltaic system

The solar PV system consists of different components that must be selected according to the type of system, the location of the site, and the applications. The main components of the solar photovoltaic system are the solar charge controller, the inverter, the group of batteries, the auxiliary power sources, and the loads (devices) as shown in Fig. 1. An installed DC/AC converter converts 48 V DC from the battery into 24 V AC as required by (low load) equipment

such as sensors, whereas a DC/DC inverter inverts the 48 V DC into 230 V AC (high load) that is used by pumps.

2.3. AGMD module

AGMD is a configuration of membrane distillation (MD) in which an air layer is interposed between a porous hydrophobic membrane and the condensation surface. Fig. 2 shows the picture of the module fitted with the cassette in a plate and frame configuration and shows the layout of components in the bench-scale MD module. The cassette of the AGMD module the following specifications: hydrophobic PTFE membrane with a pore size of 0.2 μm, the thickness of 280 μm, and total membrane area: 0.2 m² [20].

In the AGMD system, seawater is circulated through the AGMD module by the pump. It is responsible for

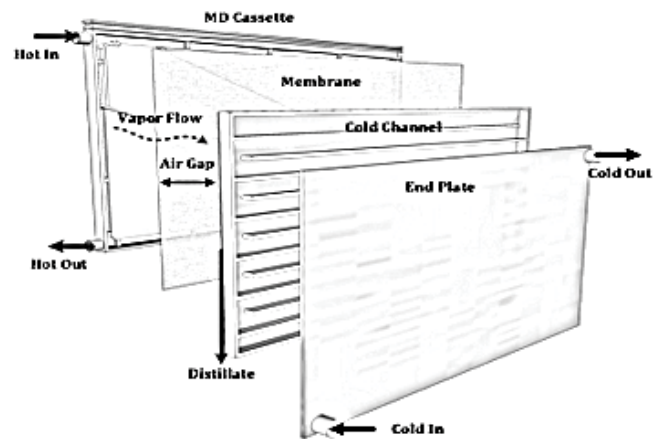


Fig. 2. Pictures of cassette fitted into the module and bench-scale AGMD module [20].

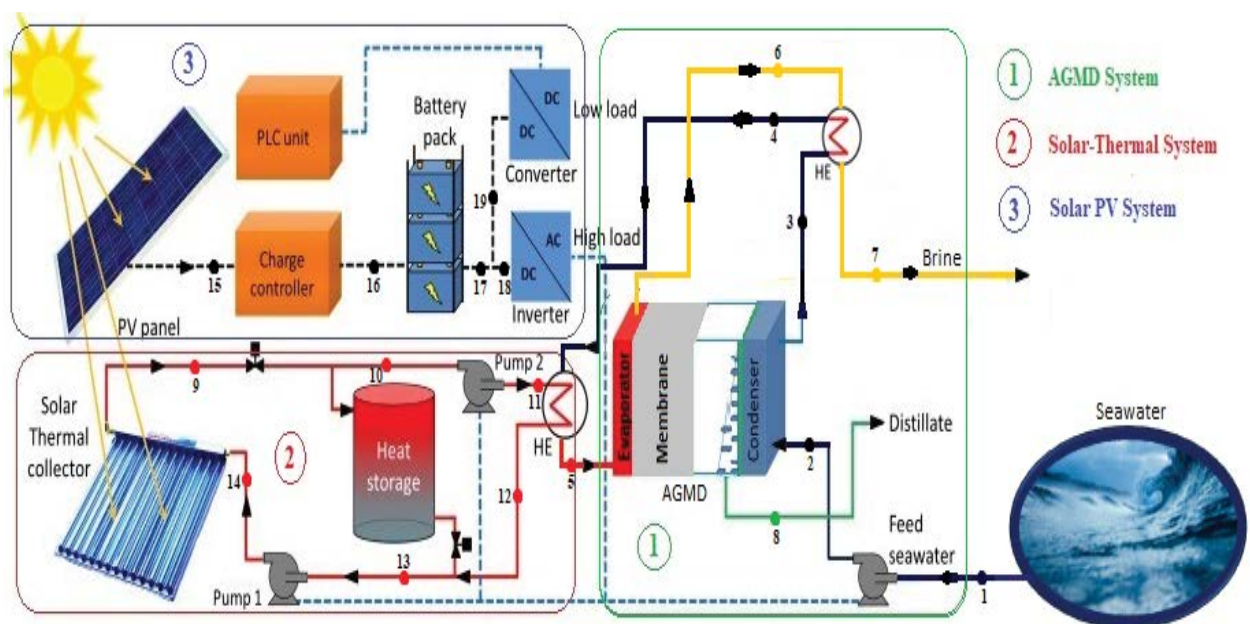


Fig. 1. Schematic of the solar AGMD system for seawater desalination.

cooling the vapor coming out from the AGMD process. The hot seawater from the AGMD process is exchanged using the thermal system via a counter-flow heat exchanger. However, to avoid losing the heat energy coming out from the evaporator, another recovery exchanger is added. Therefore, it is used to give heat energy to the cold seawater coming from the pump. However, the high salt concentration damages the distillation membrane and reduces the distilled water flow. Therefore, the saltwater leaves the membrane, and cannot returns to the process of distillation (in membrane). Furthermore, from this water we recover the remaining heat via an additional heat exchanger. Thus, the brine that contains the high salt concentration is completely dispensed with this AGMD process as shown in Fig. 1.

In addition, the salt rejection in the membrane distillation process remains high and greater than 99.9% in all cases. An experimental study was conducted to evaluate the performance of the membrane distillation in the work's Noor et al. [26]. A high saline water feed of up to 200 g/L NaCl was used in this study at various operating conditions by changing the feed temperature and feed concentration. The results estimated showed excellent conformity with the experimental results. The salt rejection remained high (greater than 99.9%) in all cases.

2.4. Weather data

This model has been studied in Ain Temouchent weather, Fig. 3 shows changing climate conditions throughout the year. The weather in Ain Temouchent state is pleasant, warm, and moderate in general. At an average temperature of 25.7°C, August is the hottest month of the year. At 10.8°C on average, January is the coldest month of the year. Therefore, in Fig. 3, we notice a change in temperature throughout the year, which reaches up to 40 degrees Celsius in August, and we note that the wind is moderate and does not exceed the velocity of 15 m/s. For the

irradiation, it changes during the months of the year and reaches up to 220 kWh/m² in August and July as shown in Fig. 4, because the temperature is high in this period of the year. This study has been simulating for a full year and the results will appear on different days in Ain Temouchent weather affected by the Mediterranean Sea.

3. Equations and methods

The most significant influential design variables on the AGMD performance are the feed inlet temperature (T_{Hin}), the cooling inlet temperature (T_{Cin}) which is condensation temperature, the feed flow rate (V_f), and feed concentration (C_f). The selected performance indicators of the AGMD process are distillate flux (J_d) and specific performance ratio (SPR), whereas J_d is calculated by [20]:

$$J_d = \frac{M_d}{S \cdot t} \quad (1)$$

where M_d (kg) is the mass of distillate water collected within the time t , and S (m²) is the effective membrane surface area of evaporation. SPR is obtained by [20]:

$$SPR = \frac{M_d}{Q_{md}} \quad (2)$$

Q_{md} (KWh) is the thermal energy supplied to the AGMD module. The regression quadratic model with coded parameters [20] can be expressed as:

$$Y = \beta_0 + \beta_1 X_1 + \beta_2 X_2 + \beta_3 X_3 + \beta_{12} X_1 X_2 + \beta_{13} X_1 X_3 + \beta_{23} X_2 X_3 + \beta_{11} X_1^2 + \beta_{22} X_2^2 + \beta_{33} X_3^2 \quad (3)$$

Kumar and Martin [20] determined the final regression equations for J_d and T_{Hout} in terms of actual operating parameters as follows:

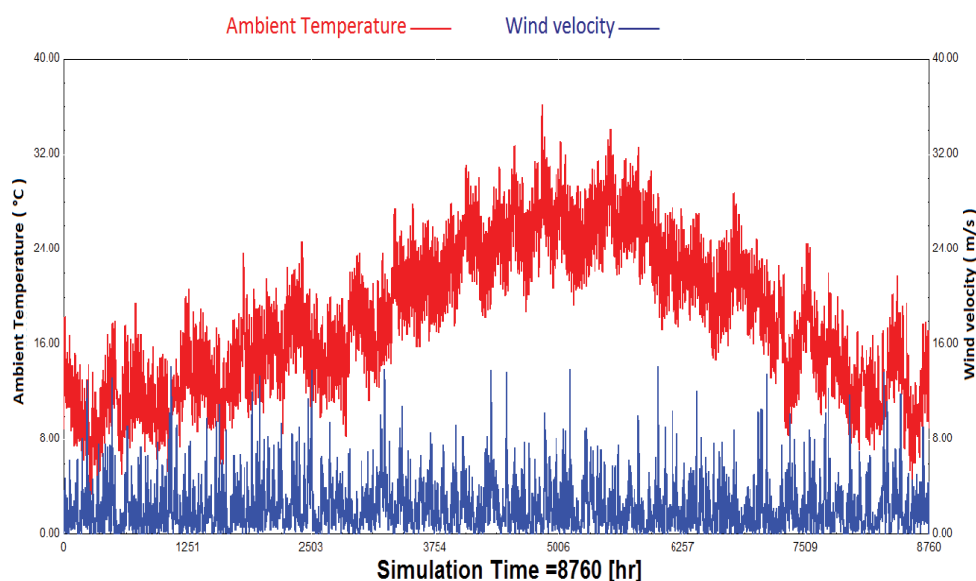


Fig. 3. Ambient temperature and wind velocity throughout the year in Ain Temouchent weather.

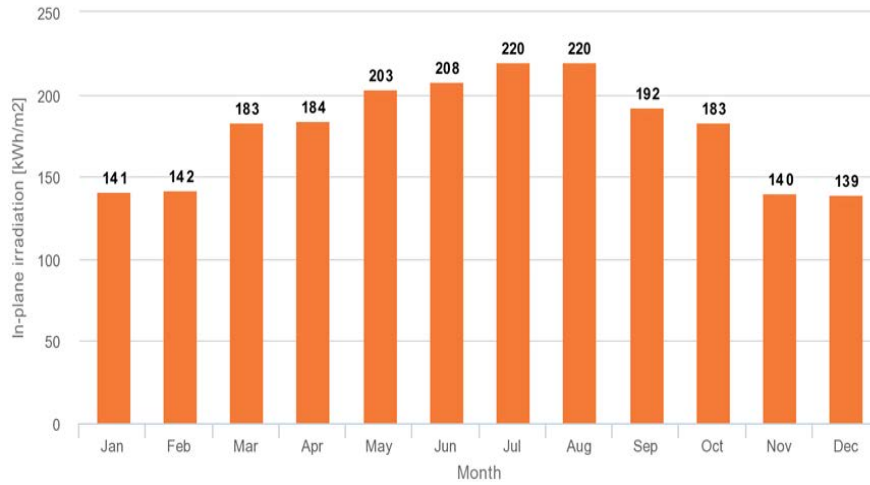


Fig. 4. Irradiation throughout the year in Ain Temouchent weather.

$$J_d = -6.57 + 0.16T_{Cin} + 0.15T_{Hin} - 5.86 \times 10^{-3}V_f - 5.77 \times 10^{-3}T_{Cin}T_{Hin} - 2.5 \times 10^{-4}T_{Cin}V_f + 3.44 \times 10^{-4}T_{Hin}V_f + 2.48 \times 10^{-3}T_{Hin}^2 \quad (4)$$

$$T_{Hout} = 3.097 + 6.82 \times 10^{-2}T_{Cin} + 0.772T_{Hin} + 3.5 \times 10^{-3}V_f + 1.42 \times 10^{-3}T_{Cin}T_{Hin} \quad (5)$$

The basic method of measuring collector performance is to expose the operating collector to solar radiation and measure the fluid inlet and outlet temperatures and the fluid flow rate. The useful gain is:

$$\dot{Q}_u = \dot{m}_0 C_{pf} (T_o - T_i) \quad (6)$$

\dot{m}_0 is the solar fluid mass flow rate (kg h^{-1}), C_{pf} is the specific heat capacity of solar fluid (kJ h^{-1}), T_o and T_i are the inlet and outlet temperature of the solar fluid (K).

The efficiency of flat plate collectors is expressed as follows [27]:

$$\eta = \eta_0 - a_0 \frac{(T - T_{amb})}{G} - a_1 \frac{(T - T_a)^2}{G} \quad (7)$$

with G the solar flux, T_a the ambient temperature, a_0 and a_1 ($\text{W m}^{-2} \text{K}^{-2}$) are characteristic constants of the efficiency of the collector.

Heat exchanger counter flow effectiveness is [22]:

$$\varepsilon = \frac{1 - \exp\left(-\frac{UA}{C_{min}}\left(1 - \frac{C_{min}}{C_{max}}\right)\right)}{1 - \left(\frac{C_{min}}{C_{max}}\right) \exp\left(-\frac{UA}{C_{min}}\left(1 - \frac{C_{min}}{C_{max}}\right)\right)} \quad (8)$$

UA is the overall loss coefficient between the heater and its surroundings during operation (kg h^{-1}), C_{max} is the maximum capacity rate ($\text{kJ h}^{-1} \text{K}$), C_{min} is the minimum capacity rate ($\text{kJ h}^{-1} \text{K}$).

Required heating rate including efficiency effects in the auxiliary heaters is [22]:

$$Q_{aux} = Q_{loss} + Q_{fluid} \quad (9)$$

with

$$Q_{loss} = UA(\bar{T} - T_{env}) + (1 - \eta_{htr})Q_{max} \text{ and } Q_{fluid} = \dot{m}_0 C_{pf} (T_{set} - T_i) \quad (9a)$$

Q_{aux} is the required heating rate including efficiency effects (kg h^{-1}), Q_{fluid} is the rate of heat addition to fluid stream (kg h^{-1}), Q_{loss} is the rate of thermal losses from the heater to environment (kg h^{-1}), Q_{max} is the maximum heating rate of the heater (kg h^{-1}), η_{htr} is an efficiency of the auxiliary heater, \dot{m}_0 is the outlet fluid mass flow rate (kg h^{-1}), C_{pf} is the fluid specific heat (kJ h^{-1}), T_i is the fluid inlet temperature (K), (\bar{T}) brackish water average temperature T_{set} set temperature of heater internal thermostat (K), T_{env} is the temperature of heater surroundings for loss calculations (K).

MD system determines the distillate water flow rate along with MD hot side outlet temperature. Other main components of the solar thermal MD system are the solar collectors, a heat exchanger, three pumps, and a hot water storage tank. The heat exchanger transfers heat from the collectors to the MD feed water stored in a small tank and it circulates to the MD module using the pumps. Cold-water pumps to MD from a cold-water storage tank having temperatures according to the ambient conditions of the location. Table 1 shows the main specifications considered for the components of the solar thermal MD system. Five flat plate collectors having a total area of 12.75 m^2 considered for both experiments and the simulation model. A simple storage tank with fixed inlets and uniform heat losses use for feeding water storage. The temperature differential controller uses to control the flow of heat transfer fluids in the solar thermal system. This model studies throughout the year, especially in December when the minimum radiation is incident on solar collectors in Ain Temouchent.

Table 1
Main specifications for the solar thermal integrated MD system [20]

Component	Parameter	Value	Unit
Flat plate collectors	Collector absorber area	12.75	m ²
	Collector efficiency	0.781	–
	Tilt angle	35	°
Heat exchanger	Effectiveness	0.5	–
MD hot water store	Volume	100	L
MD hot pump	Flow rate	420	kg h ⁻¹
Auxiliary heaters	Maximum heating rate	1,500	W
	Efficiency of the auxiliary heater	1	–

The use of solar energy considerably reduces operating costs; however, its intermittent nature requires a non-stationary optimal operation that can be achieved through advanced control strategies. In this study, the control and the thermal system for the MD process make with the use of photovoltaic panels for cost savings. Therefore, to reduce the operating cost, the photovoltaic system uses a storage battery that replaces the power load of the pumps, which appears in Fig. 2. Then, the following output parameters, which are the outlet temperature of the solar collector and auxiliary power supplied to the storage tank. The control and the thermal system for the MD process also make with the use of photovoltaic panels device for cost savings. In this study, a TRNSYS program and PVGIS software are used to predict the long-term performance of the solar water heating systems in different locations for the distillation membrane, and they can simulate the system performances under different weather, among them the operating conditions in the weather of the state Ain Temouchent, Algeria.

The PV system is calculated based on the parameters of Table 2 using PVGIS software and the following equations:

The peak power of the autonomous photovoltaic installation

$$P_c = P_{pv} = \frac{D}{N \times F} \tag{10}$$

P_c power of the PV field, D daily need kWh/h, F form factor, N number of hours equivalent.

$$N = \frac{G_T(t)}{G_{T,STC}} \tag{11}$$

$G_T(t)$ is the solar radiation incident on the solar_PV array in the current time step kW/m².

$G_{T,STC}$ is the incident radiation at standard test conditions kW/m².

The size of the inverter from 25% to 30% must be greater than the total quantity of devices. In the case of a device or compressor, the size of the inverter must be at least 3 times the capacity of these devices and must be added to the capacity of the inverter to handle the surge current during startup.

The storage capacity of the battery is calculated according to the following relation [28,29]:

$$C(\text{Wh}) = \frac{D \times 1000 \times N_j}{n_b \times P_d \times P_r} \tag{12}$$

D daily need, N_j autonomy number of days without radiation, n_b battery efficiency, $P_r = (1 - \text{online losses})$, P_d Depth of the discharge.

The bulk temperature of the feed is used for calculating the latent heat of evaporation. The thermal efficiency of the MD unit is given by [30]:

$$EE = \frac{m_p \times H_v}{Q_{in}} \tag{13}$$

Table 2
Technical characteristics of PV panels

Component	Parameter	Value	Unit
PV panel	Module area	1.6	m ²
	Power tolerance	±5	%
	Solar cells	36	Cells
	Module open-circuit voltage at reference conditions	38.9	V
Battery	Module short-circuit voltage at reference conditions	9.31	Amperes
Inverter	Tolerance for iterative calculations	16.7	Ah
	Charging efficiency	0.8	–
	High limit on the fractional state of charge (FSOC)	1	–
	Regulator efficiency	0.78	–

$$Q_{in} = m_f \times C_p \times (T_{feed,in} - T_{feed,out}) \tag{14}$$

where m_f is the feed-water flow rate (kg/h), C_p is the feed-water heat capacity (kWh/kg°C), $T_{feed,in}$ is the evaporator inlet temperature (°C) and $T_{feed,out}$ is the evaporator outlet temperature (°C).

Where H_v is latent heat of vaporization (J/kg) [26], m_p is permeate flux (kg/s), H_v is estimated by [26]:

$$H_v = 2501.897149 - 2.407064037T + 0.001192217T^2 - 0.000015863T^3 \tag{15}$$

where T is the average temperature at the evaporator entrance and the exits of the condenser (°C).

In addition, in this study with these equations, a TRNSYS program is used to predict the long-term performance of the solar water heating system for the AGMD process. A complete test rig to evaluate the performance of membrane distillation module is driven by solar energy using the flat plate collectors in Ain Temouchent weather, Algeria. Where Ain Temouchent is near the north coast of Algeria affected by the Mediterranean Sea.

4. Solar AGMD system in the TRNSYS simulation

The model of solar thermal membrane distillation system with AGMD and the photovoltaic system is developed using TRNSYS software, which is a quasi-steady-state simulation program. TRNSYS enables system components represented as preformats to be selected and interconnected in any desired manner to construct a system's

model. To facilitate the selection of the system components, it is important to develop an information flow diagram. The information flow diagram for the models is shown in Fig. 5. The main component of the model is the AGMD unit, which is represented by a new equation in TRNSYS. Additional components to the model include TYPE109–TM2 reading and processing of meteorological data, Type 91 heat exchanger, Type 1 flat plate collector, Type 2 differential temperature controller, Type 3 single speed pump, Type 94 photovoltaic panels, Type 47 storage battery, Type 48 inverter, Type 14 forcing functions, Type 57 unit conversion and Type 65 online plotter. Tables 1 and 3 show the values of parameters used in the TRNSYS model.

5. Results and discussion

5.1. Model validation

The aim of this section is the validity of input data and output results under the same operating conditions for the AGMD module in order to obtain correct and accurate results. Fig. 6 shows the comparison between the

Table 3
Operational conditions of tested AGMD module [20]

Operational parameter	Specification
Feed flow rate, L/min	4, 6 and 8
Hot water operation temperature, °C	40–90
Coldwater operation temperature, °C	10–50
Tap water conductivity, µS/cm	500–10,000

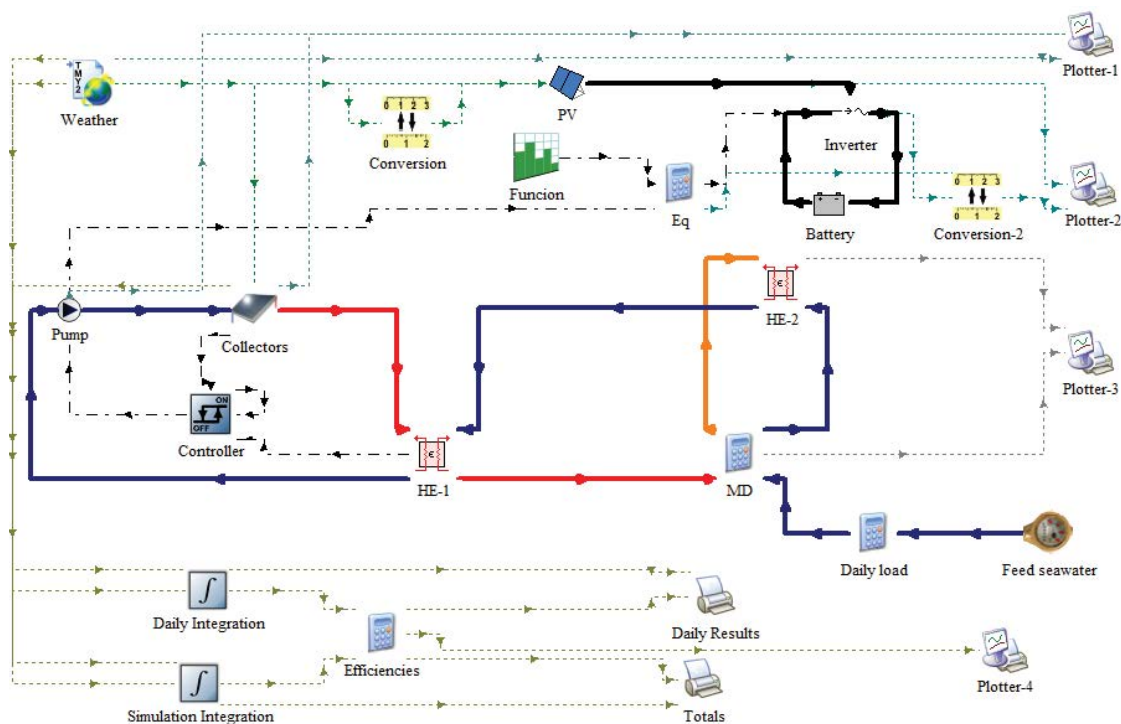


Fig. 5. Diagram of the solar AGMD system in the TRNSYS program.

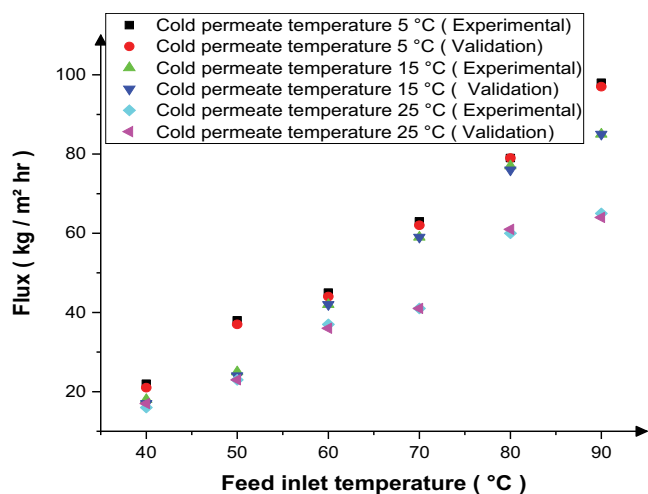


Fig. 6. Effect of feed inlet temperature on flux [20].

experimental results and the simulated results obtained from the model used. Then, it presents the effect of inlet feed temperature on permeate flux, the feed temperature varies from 40°C to 90°C. The system runs under the following operating conditions: hydrophobic PTFE membrane with a pore size of 0.2 μm , the thickness of 280 μm , total membrane area: 0.2 m^2 , permeate flow rate of 3.65 L/min, and feed flow rate of 4.65 L/min with feed salinity of 2 g/L. As shown in Figs. 6–8, it can be noticed that the hot and cold feed outlet temperatures and permeate flux of the AGMD module calculated by the present model have good compatibility of no more than 5% in this experiment. This good compatibility using the TRNSYS program on the experimental AGMD system installed in the UAE [20] makes it suitable for use in various climatic changes like Ain Temouchent weather in Algeria, which is characterized by a good solar climate. The results show that increasing the feed inlet temperature increases the system flux significantly. Increasing the feed inlet temperature increases the vapor production and the driving force to permeation (the transmembrane temperature difference, and consequently the difference in partial pressures across membrane surfaces) which enhance permeation across the membrane. The percentage increase in flux when the feed temperature is increased from 40°C to 90°C is 56% at permeate temperature of 25°C, 41% at 15°C, and 30% at 5°C as shown in Fig. 6. Thus, percentagewise, higher cold permeate temperature gives more percentage increase in flux.

Fig. 7 shows the comparison of the inlet hot feed side temperature of the AGMD module between the given experiment results [20] and the simulated results obtained from the model used. It can be noticed that the inlet hot feed side temperature of the AGMD module predicted by the present model has a good agreement with the experiment. The outlet temperature of the thermal system of an AGMD module reaches 84°C in the maximum radiation from October on solar collectors in UAE. Based on this result as shown in Fig. 7, the present study aims at simulating the solar-based solar thermal membrane distillation system considered as a field trial installation in UAE.

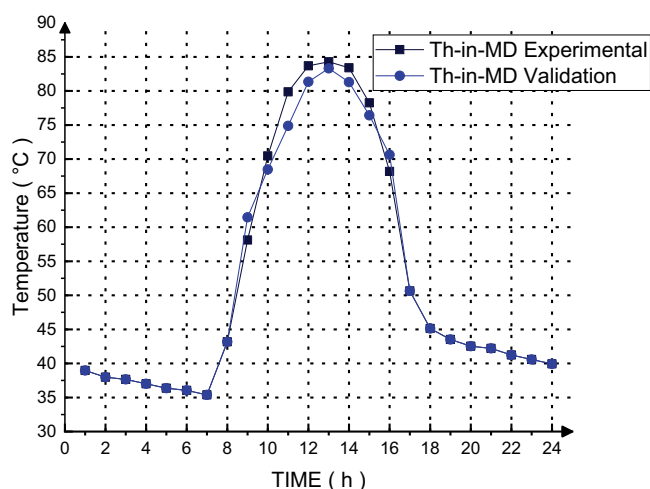


Fig. 7. Comparison of temperature outlet of the thermal system between the simulation and the experimental data [20].

In Fig. 8, a single cassette AGMD module is studied to identify the effect of process parameters on distillate flux. Fig. 8 shows a comparison between the results of this simulation and the applied results from Kumar and Martin's article [20]. The results show excellent compatibility between them. This agreement using the experimental parameters of the article by Kumar and Martin [20] confirms the validity of this system studied in this paper. This is shown by the distillation flow rate value. Therefore, favorable conditions were determined and validated to obtain a distillate flow rate of 4.5 kg/h.

Based on the experimental characteristics of the AGMD module, the simulation results are validated with experimental data obtained from the pilot solar thermal membrane distillation system mounted in UAE [20].

5.2. Thermal capacity and permeate flux

Fig. 9 shows the outlet temperatures for five flat plate collectors that have a total area of 12.75 m^2 considered for both experiments and the simulation model. It is found that the change in feed inlet temperature of AGMD module profiles for the first day of January, April, August, and November is illustrated in Fig. 9. The temperature decreases in January and reaches 78°C, but it increases in August when the temperature is high and reaches 95°C, as it reaches 84°C and 82°C respectively in April and November. This change is due to the change in ambient temperature and radiation in the daytime and their difference from month to month. Therefore, plots show a remarkable influence of the hot feed temperatures during the days of winter and summer seasons by the percentage reaches 18%.

Fig. 10 shows the inlet feed temperatures of AGMD coming from the exchanger heaters and using the flat plate collectors. The system runs under the following operating conditions: hydrophobic PTFE membrane with a pore size of 0.2 μm , the thickness of 280 μm , total membrane area: 0.2 m^2 , and permeate flow rate of 3.65 L/min, the feed flow rate of 4.65 L/min with feed salinity of 2 g/L. The inlet feed temperatures reach 70°C and 74°C in January and November,

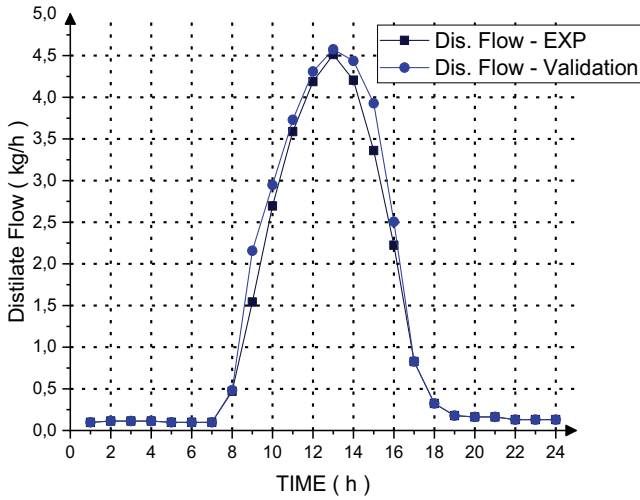


Fig. 8. Comparison of distillate flow between the simulation and the experimental data [20].

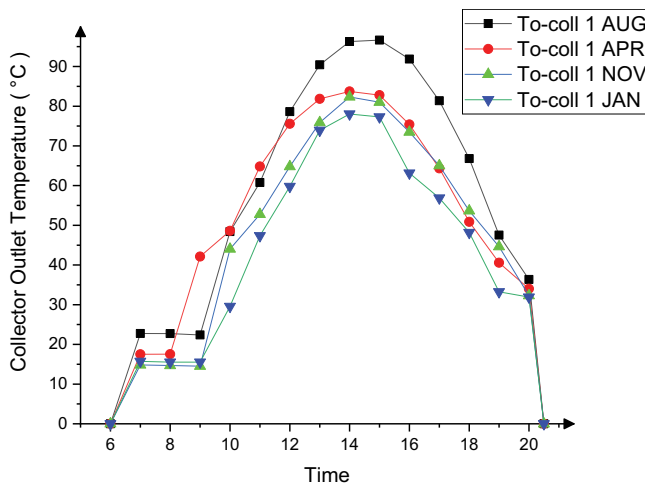


Fig. 9. Distribution of collector outlet temperature along the day during four seasons.

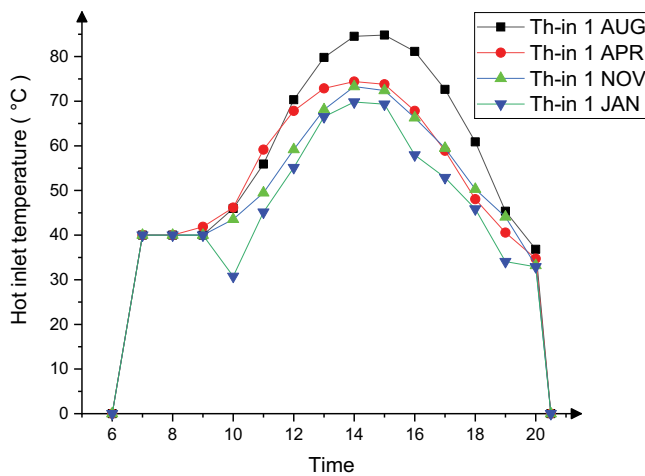


Fig. 10. Distribution feed inlet temperature of AGMD.

as it reaches 75°C and 85°C in April and August respectively. Therefore, it can be seen that the percentage increases in the high temperature during the days of winter and summer seasons by the percentage, 17.8%.

Fig. 11 shows the variation of permeate flux variation with keeping all other parameters constant as above. Clearly, the trends show that the permeate flux increases with various intermittent climatic conditions. Therefore, the inlet hot temperature is very effective to increase the permeate flux at different times as shown in Fig. 11. It is worth mentioning that the exponential nature of flux increase can better be observed in summer as compared to other times. Over the entire range of permeate flux (3–5 L/h) and throughout the year, the percentage increases in flux and reaches 40% between winter and summer.

5.3. Power to load of the photovoltaic system

To save costs, a photovoltaic system uses based on renewable energy (solar energy). Therefore, the energy needed calculates for the pumps and replaces by two photovoltaic panels, each one has an area of 1.6 m² using an energy storage battery (12 V, 200 Ah) via TRNSYS and PVGIS help programs. Accordingly, the purpose of this study is the use of solar panels in the photovoltaic system to produce the necessary electrical energy. Therefore, we note in Fig. 12 that the electric power of the pumps that reaches 0.2 kW is the same energy that comes out of the photovoltaic system. Consequently, the electrical energy of the pumps is replaced by using the PV system panels in various intermittent climatic conditions as shown in Fig. 12.

5.4. Flat plate thermal solar collector efficiency

Fig. 13 shows the four efficiencies for the evolution of the entire year. The results show that the efficiencies increase from 0.65 to 0.74 during summer, as they reach 0.59, 0.63, and 0.64 respectively in January, November, and April. Therefore, the changing climate conditions throughout the year are very effective in increasing the flat plate

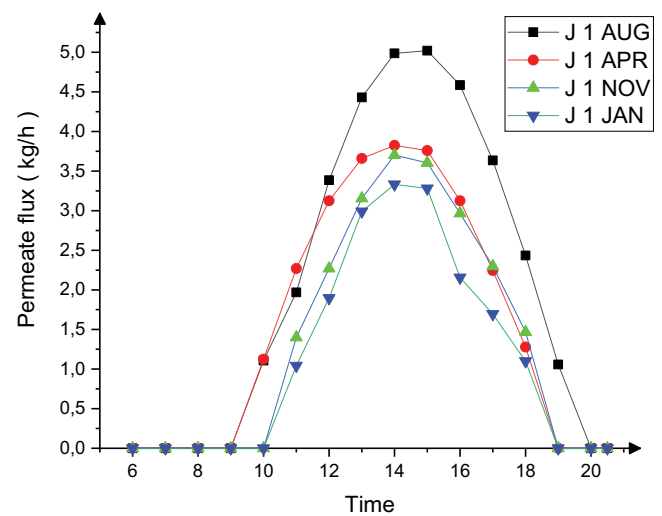


Fig. 11. Permeate flux of AGMD.

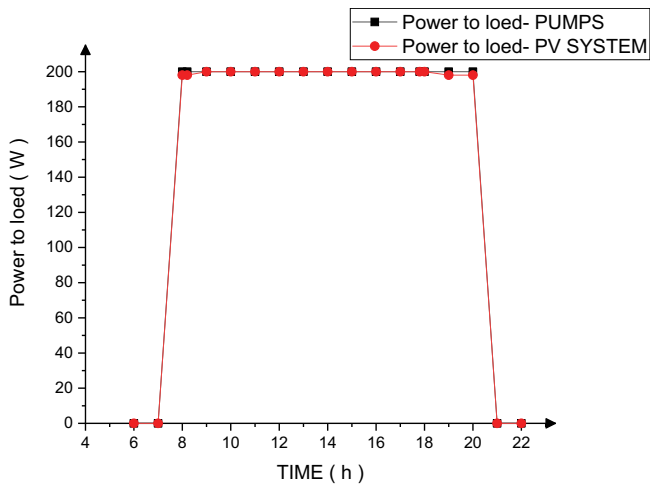


Fig. 12. Power to load of the PV system and pumps for the AGMD system.

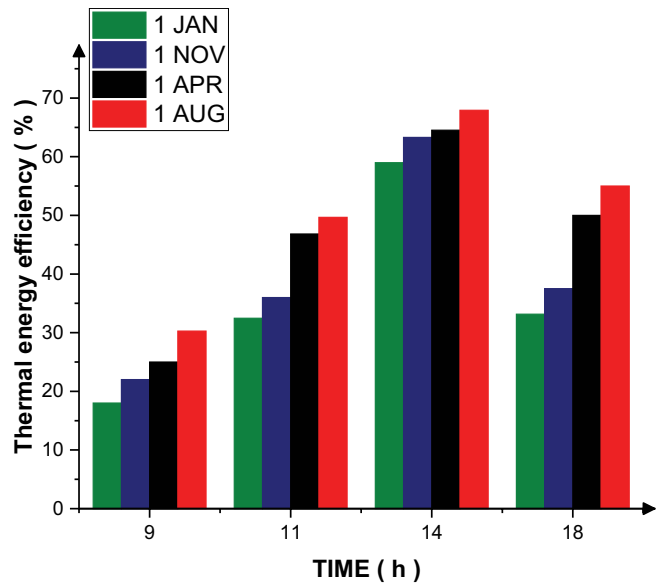


Fig. 14. The thermal energy efficiency of the AGMD module during 4 d.

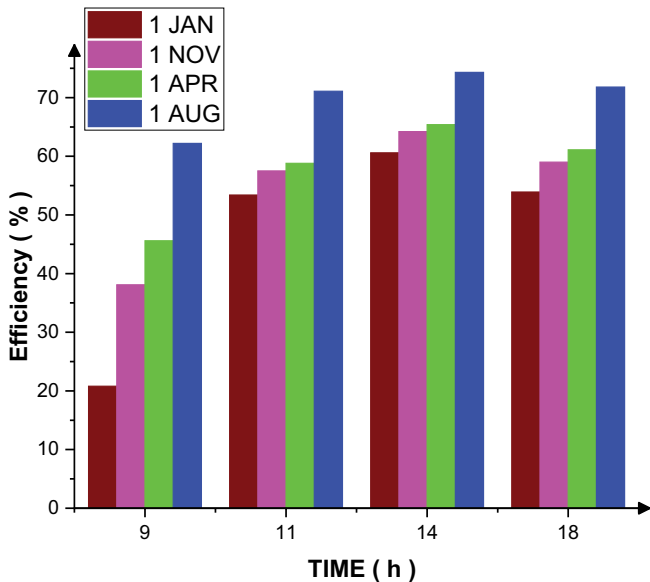


Fig. 13. The flat plate thermal solar collector efficiency during 4 d.

thermal solar collector efficiencies. Percentagewise, the efficiencies increase from 18.4% to 66.6% throughout the entire year.

5.5. Thermal energy efficiency of the AGMD system

Fig. 14 shows the effect of the thermal energy efficiency of the AGMD module on different days of the year. The changing climate conditions are varied from winter to summer while keeping all other parameters constant as mentioned in Table 1. As shown in Fig. 13 and by percentage, the energy efficiency increases by 67.2% between winter and summer. Over the entire range of time (throughout the year) 40.6% increase in the energy efficiency is obtained at 9 h, 34.7% is obtained at 11 h, 13.2% is obtained at 14 h and 39.7% is obtained at 18 h. Therefore, increasing the

temperatures with the changing climate conditions every day from the year increases the thermal energy efficiency of the AGMD module. Thus, it increases the difference in partial pressure that assists the permeation process across the membrane.

6. Conclusion

A complete test rig to evaluate the performance of membrane distillation module is driven by solar energy during the flat plate collectors heating process is simulated in Ain Temouchent, Algeria.

Optimized parametric conditions were used to operate the solar thermal driven membrane distillation system in Ain Temouchent City and the system was simulated using the TRNSYS tool. The AGMD numerical data is validated using a multiple regression model relating to the operating parameters of the solar AGMD system. As shown in Figs. 6–8, It can be noticed that the hot and cold feed outlet temperatures and permeate flux of the AGMD module calculated by the present model have good compatibility of no more than 5% in this experiment. Therefore, the dynamic simulation results of the solar AGMD system show good agreement with the experimental values.

In addition, the results showed the permeate flux of the AGMD module using the FPC module throughout the year. It was observed that the effect of flow rates of feed inlet and hot temperature in AGMD is very effective to increase the permeate flux. Distillate flux was varied from 3 to 5 kg/h in various intermittent climatic conditions. Based on the numerically characterized AGMD module, the results show that increasing the feed inlet temperature increases the system flux significantly. Increasing the feed inlet temperature increases the vapor production and the driving force to permeation (the transmembrane temperature difference, and consequently the difference in partial pressures across membrane surfaces) which enhances permeation across the

membrane. Higher values are achieved with high hot feed temperature and flow rates. The energy efficiency of the AGMD module and the collector efficiency values reach 68% and 74% respectively. The interaction effects between all the input parameters are evident in modeling the distillate flux whereas for efficiencies high variations are observed due to the interaction effects of the feed inlet temperature and changing climate conditions throughout the year in Ain Temouchent weather. Besides, the brine that contains the high salt concentration is completely dispensed with this process.

The simulation results show that a very simple AGMD system with a total collectors area of 12.75 m² for the production of 3–5 L/h of distilled water flow throughout the entire year. To save costs, a photovoltaic system uses depending renewable energy (solar energy). Therefore, the energy needed calculates for the pumps and replaces by two photovoltaic panels, each one has an area of 1.6 m² using an energy storage battery (12 V, 200 Ah) via TRNSYS and PVGIS help programs. Accordingly, the purpose of this study is the use of solar panels in the photovoltaic system to produce the necessary electrical energy. The AGMD system using solar energy for seawater desalination will be useful for further simulations or applications of the technology. Finally, these types of projects that integrate renewable energy technologies with additional services are in principle attractive in terms of the associated socio-economic benefits.

Acknowledgments

The authors would like to express their gratitude to Professors N.T. Uday Kumar and Andrew Martin. We would also like to thank our friends and family who supported me and offered deep insight into the study. We wish to acknowledge the help provided by the technical and support staff in the Smart Structures Laboratory of the University Ain Temouchent Belhadj Bouchaib.

Symbols

C_{pf}	—	Specific heat capacity of solar fluid, kJ/h
V_f	—	Feed flow rate, kg/h
J_d	—	Distillate flux, kg/h
T	—	Temperature, °C
M_d	—	Mass of distillate water, kg
S	—	Effective membrane surface area of evaporation, m ²
Q_{md}	—	Thermal energy supplied, kWh
t	—	Time, h
m_0	—	Solar fluid mass flow rate, kg/h
UA	—	Overall loss coefficient between the heater and its surroundings during operation, kg/h
C	—	Capacity rate, kJ/h K
Q	—	Heating rate of the heater, kg/h
\bar{T}	—	Brackish water average temperature, K
T_{set}	—	Set temperature of heater internal thermostat, K
T_{env}	—	Temperature of heater surroundings for loss calculations, K
P_c	—	Power of the PV field
D	—	Daily need, kWh/d
F	—	Form factor

N	—	Number of hour's equivalent
$G_T(t)$	—	Solar radiation incident on the solar-PV array in the current time step, kW/m ²
$G_{T,STC}$	—	Incident radiation at standard test conditions, kW/m ²
N_j	—	Autonomy number of days without radiation
P_j	—	Discharge

Greek

ε	—	Heat exchanger counter flow effectiveness
η	—	Efficiency

Subscripts

in	—	Inlet
out	—	Outlet
h	—	Hot
c	—	Cold
p	—	Permeate
d	—	Depth
hr	—	Hour
loss	—	Losses
max	—	Maximum
min	—	Minimum

References

- [1] M.T. Ali, H.E.S. Fath, P.R. Armstrong, A comprehensive techno-economical review of indirect solar desalination, *Renewable Sustainable Energy Rev.*, 15 (2011) 4187–4199.
- [2] J. Phattaranawik, R. Jiratananon, A. Fane, Heat transport and membrane distillation coefficients in direct contact membrane distillation, *J. Membr. Sci.*, 212 (2003) 177–193.
- [3] M. Teoh, T. Chung, Membrane distillation with hydrophobic macrovoid-free PVDF-PTFE hollow fiber membranes, *Sep. Purif. Technol.*, 66 (2009) 229–236.
- [4] R.W. Schofield, A.G. Fane, C.J. Fell, Heat and mass transfer in membrane distillation, *J. Membr. Sci.*, 33 (1987) 299–313.
- [5] A. Boubakri, A. Hafiane, S.A.T. Bouguecha, Direct contact membrane distillation: capability to desalt raw water, *Arabian J. Chem.*, 10 (2017) 75–81.
- [6] A.K. Thakur, I.M. Hsieh, M.R. Islam, B. Lin, C.C. Chen, M. Malmali, Performance of sweeping gas membrane distillation for treating produced water: modeling and experiments, *Desalination*, 492 (2020) 554–597.
- [7] A. Alkudhiri, N. Darwish, N. Hilal, Membrane distillation: a comprehensive review, *Desalination*, 287 (2012) 2–18.
- [8] R. Ullah, M. Khraisheh, R.J. Esteves, J.T. McLeskey, A.-S. Jönsson, G. Mohamed, H.V. Tafreshi, Energy efficiency of direct contact membrane distillation, *Desalination*, 433 (2018) 56–67.
- [9] M. Qtaishata, T. Matsuura, B. Kruczek, M. Khayet, Heat and mass transfer analysis in direct contact membrane distillation, *Desalination*, 219 (2008) 272–292.
- [10] G.L. Hassler, U.S. Patent US3129146A (14 April 1964).
- [11] P.K. Weyl, U.S. Patent US3340186A (5 September 1967).
- [12] A.-S. Jönsson, R. Wimmerstedt, A.-C. Harrysson, Membrane distillation – a theoretical study of evaporation through microporous membranes, *Desalination*, 56 (1985) 237–249.
- [13] C. Gostoli, G.C. Sarti, S. Matulli, Low temperature distillation through hydrophobic membranes, *Sep. Purif. Technol.*, 22 (1987) 855–872.
- [14] F.A. Banat, F.A. Al-Rub, R. Jumah, M. Shannag, Theoretical investigation of membrane distillation role in breaking the formic acid-water azeotropic point: comparison between Fickian and Stefan-Maxwell-based models, *Int. Commun. Heat Mass Transfer*, 26 (1999) 879–888.

- [15] J. Swaminathan, H.W. Chung, D.M. Warsinger, F.A. AlMarzooqi, H.A. Arafat, Energy efficiency of permeate gap and novel conductive gap membrane distillation, *J. Membr. Sci.*, 502 (2016) 171–178.
- [16] A.M. Alklaibi, N. Lior, Membrane-distillation desalination: status and potential, *Desalination*, 171 (2005) 111–131.
- [17] L. Camacho, L. Dumée, J. Zhang, J.-d. Li, Duke, J. Gomez, S. Gray, Advances in membrane distillation for water desalination and purification applications, *Water*, 5 (2013) 94–196.
- [18] E.U. Khan, A.R. Martin, Water purification of arsenic-contaminated drinking water via air-gap membrane distillation (AGMD), *Period. Polytech., Mech. Eng.*, 58 (2014) 47–53.
- [19] Q. He, P. Li, H. Geng, C. Zhang, J. Wang, H. Chang, Modeling and optimization of air-gap membrane distillation system for desalination, *Desalination*, 354 (2014) 68–75.
- [20] N.T. Uday Kumar, A. Martin, Experimental modeling of an air-gap membrane distillation module and simulation of a solar thermal integrated system for water purification, *Desal. Water Treat.*, 84 (2017) 123–134.
- [21] M. Asim, N.T. Uday Kumar, A. Martin, Feasibility analysis of solar combi-system for simultaneous production of pure drinking water via membrane distillation and domestic hot water for single-family villa: pilot plant setup in Dubai, *Desal. Water Treat.*, 57 (2015) 21674–21684.
- [22] N.T. Uday Kumar, A. Martin, Techno-economic optimization of solar thermal integrated membrane distillation for co-generation of heat and pure water, *Desal. Water Treat.*, 98 (2017) 16–30.
- [23] M. Gowtham, N.T. Uday Kumar, P.K. Manoj, A. Martin, A novel solar thermal polygeneration system for sustainable production of cooling, clean water and domestic hot water in United Arab Emirates: dynamic simulation and economic evaluation, *Appl. Energy*, 167 (2016) 173–188.
- [24] TRNSYS, Transient System Simulation, Univ. Wisconsin Madison, WI: Solar Energy Sci. Laboratory, 2 (2017) 1–129.
- [25] PVGIS, Photovoltaic Geographical Information System, JRC European Commission, Joint Research Center 2007.
- [26] A.M.A. Noor, S.S. Ibrahim, Q.F. Alsathy, A. Figoli, Highly saline water desalination using direct contact membrane distillation (DCMD): experimental and simulation study, *Water*, 12 (2020) 15–75.
- [27] A. Remlaoui, D. Nehari, M. Laissaoui, A. Marni Sandid, Performance evaluation of a solar thermal and photovoltaic hybrid system powering a direct contact membrane distillation: TRNSYS simulation, *Desal. Water Treat.*, 194 (2020) 37–51.
- [28] A.R. Aguirre, J.A.A. Mañas, J.M.F. Sevilla, G. Zaragoza, Experimental characterization and optimization of multi-channel spiral wound air-gap membrane distillation modules for seawater desalination, *Sep. Purif. Technol.*, 205 (2018) 212–222.
- [29] A.N. Mabrouk, Y. Elhenawy, M. Abdelkader, M. Shatat, The impact of baffle orientation on the performance of the hollow fiber membrane distillation, *Desal. Water Treat.*, 58 (2017) 35–45.
- [30] J. Koschikowski, M. Wieghaus, M. Rommel Solar thermal-driven desalination plants based on membrane distillation, *Desalination*, 156 (2003) 295–304.